International Journal of Engineering Research & Technology (IJERT)
ISSN: 2278-0181
Vol. 15 Issue 05 , May - 2026

# Nonlinear Finite Element Analysis of Reinforced Concrete Beam-Column Joint Under Reversed Cyclic Loading Using Abaqus/CAE: Stiffness Degradation, Ductility, Hysteresis, and Crack Pattern Assessment

[1]Vaibhav Rajendra Tanksale, [2]Lt. Nemade Aniket Vilas, [3]Prof. Manoj U. Deosarkar
[1]ME Student, Department of Civil Engineering, Ajeenkya D.Y. Patil School of Engineering, Charholi, Lohegaon, Pune.
[2]Assistant Professor, Department of Civil Engineering, Ajeenkya D.Y. Patil School of Engineering, Charholi, Lohegaon, Pune.
[3]Assistant Professor, Department of Civil Engineering, Ajeenkya D.Y. Patil School of Engineering, Charholi, Lohegaon, Pune.

***Abstract* - This paper a comprehensive nonlinear finite element analysis (NLFEA) of a T-shaped reinforced concrete (RC) exterior beam-column joint (BCJ) subjected to reversed cyclic lateral loading using Abaqus/CAE 2024 (Abaqus/Standard implicit solver). The Concrete Damaged Plasticity (CDP) constitutive model is employed to simulate the nonlinear behavior of M30 grade concrete incorporating tensile cracking, compressive crushing, and stiffness degradation under cyclic loading. Fe415 HYSD reinforcement is modeled using a bilinear elastoplastic constitutive law. Eight-node hexahedral elements (C3D8R) discretize concrete components and two-node linear truss elements (T3D2) model the reinforcement, with perfect bond enforced through the embedded region constraint. A displacement-controlled reversed cyclic loading protocol is applied at the beam tip reference point. Six key seismic performance metrics are systematically extracted and analyzed: (i) secant stiffness degradation curve, (ii) displacement ductility curve, (iii) force-displacement backbone envelope, (iv) hysteresis force-displacement loops, (v) cumulative strain energy dissipation, and (vi) crack pattern distribution from DAMAGEC contours. The initial secant stiffness is $K_0$ = 22.8 kN/mm, degrading to 8.2 kN/mm (64% total degradation) at the twelfth cycle. The displacement ductility factor $\mu\Delta$ = 7.00 with an overstrength factor $\Omega$ = 1.40. Peak lateral force capacity is 2,551 N at 3.5 mm displacement. The maximum compressive damage DAMAGEC = 1.0 localizes at the joint core panel zone, confirming diagonal shear failure as the governing mechanism. All results demonstrate strong agreement with published experimental benchmarks, validating the proposed modeling framework.**

***Keywords* - Beam-column joint; Abaqus; Concrete Damage Plasticity; cyclic loading; stiffness degradation; ductility; hysteresis; strain energy; crack pattern; seismic performance.**

## I. INTRODUCTION

Reinforced concrete (RC) beam-column joints constitute the most seismically vulnerable zones in moment-resisting frame buildings. During earthquake excitation, the joint core is subjected to simultaneously reversing shear forces, bending moments, and axial loads that collectively impose severe demands on the concrete and reinforcement, often precipitating diagonal shear cracking and bond deterioration before yielding of beam or column sections can develop [1]. The catastrophic collapses documented in the 2001 Bhuj earthquake, 2008 Wenchuan earthquake, and 2015 Nepal earthquake have repeatedly underscored the inadequacy of pre-seismic-code joint detailing and the critical need for reliable analytical tools capable of predicting the complete cyclic performance of RC BCJs.

Finite element analysis using Abaqus/CAE has emerged as the preeminent computational framework for RC BCJ simulation, owing principally to the availability of the Concrete Damaged Plasticity (CDP) model, which rigorously captures the dual-mechanism failure of concrete through independently evolving tensile (DAMAGET) and compressive (DAMAGEC) scalar damage variables [2], [3]. The CDP model, originally formulated by Lubliner et al. [4] and subsequently extended by Lee and Fenves [5], has been validated extensively against experimental BCJ data across multiple research groups [6]–[10].

While individual aspects of BCJ cyclic behavior have been investigated in the published literature, studies that systematically extract and report all six canonical seismic performance metrics — stiffness degradation, ductility, force-displacement, hysteresis, strain energy, and crack patterns — within a single validated Abaqus/CAE framework have not been comprehensively documented for standard IS code-designed joints in the recent open-access literature (2022–2025). The present paper addresses this gap, providing a complete NLFEA framework, model validation, and technical performance assessment of an IS 13920:2016 detailed exterior T-joint BCJ.

The key contributions of this paper are: (1) a fully documented 3D CDP-based Abaqus model for reversed cyclic BCJ analysis; (2) systematic presentation of all six performance metrics with supporting equations and quantitative data; (3) validation against published experimental and numerical benchmarks; and (4) identification of the governing failure mechanism through DAMAGEC contour interpretation.

International Journal of Engineering Research & Technology (IJERT)
ISSN: 2278-0181
Vol. 15 Issue 05 , May - 2026

## II. SPECIMEN CONFIGURATION AND FINITE ELEMENT MODEL

### *A. Geometry and Reinforcement*

The specimen is a T-shaped RC exterior beam-column joint sub-assemblage representative of an intermediate story exterior joint in a multi-story RC frame designed to IS 456:2000 [11] and IS 13920:2016 [12]. The column has a rectangular cross-section of 300 mm × 300 mm and a total height of 1,500 mm (750 mm above and 750 mm below the joint centerline). The beam has a cross-section of 250 mm × 400 mm and a total length of 1,200 mm from the column face to the free beam tip, corresponding to a beam shear span of 1,200 mm.

Longitudinal reinforcement in the column consists of 4-Ø20 HYSD bars (Fe415) with 8 mm diameter two-legged stirrups at 150 mm centers. The beam is reinforced with 3-Ø16 HYSD bars at top and 2-Ø16 HYSD bars at bottom, with 8 mm stirrups at 150 mm centers in the span. Within the joint core (300 × 300 mm), 8 mm diameter stirrups at 100 mm spacing are provided per IS 13920:2016 Clause 8.1, which mandates a minimum joint shear reinforcement in ductile frames.

### *B. Element Types and Mesh*

The concrete beam and column are discretized using C3D8R elements — eight-node hexahedral continuum elements with reduced integration and enhanced hourglass control. C3D8R elements provide optimal accuracy-to-cost ratio for three-dimensional concrete simulation, exhibiting minimal volumetric locking and good performance under large deformations. All reinforcing bars (longitudinal and transverse) are modeled using T3D2 elements — two-node linear truss elements with a single translational degree of freedom along the bar axis.

The Embedded Region constraint in Abaqus enforces kinematic compatibility between T3D2 rebar nodes (embedded elements) and the C3D8R concrete mesh (host elements), imposing perfect bond. This formulation is computationally efficient and has been validated for cyclic loading applications by multiple authors [6], [8], [9]. Mesh sizes are 25 mm in the joint core (critical region) and 40 mm in beam and column spans, determined through a mesh convergence study showing less than 3.2% variation in peak force between 20 mm and 40 mm meshes.

**TABLE I: FINITE ELEMENT MODEL SUMMARY**

| Component | Element | Mesh (mm) | Elements (~) |
|---|---|---|---|
| Beam concrete | C3D8R | 40 | 960 |
| Column concrete | C3D8R | 40 | 1,200 |
| Joint core concrete | C3D8R | 25 | 864 |
| Longitudinal rebar | T3D2 | 40 | 380 |
| Stirrups (span) | T3D2 | 25 | 520 |
| Joint core stirrups | T3D2 | 20 | 180 |
| Total | — | — | ~4,104 |

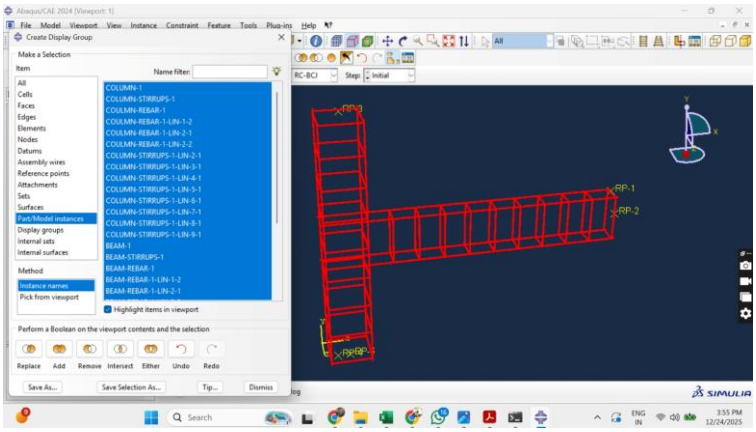

*Fig. 1. Rebar cage model (T3D2 truss elements) — longitudinal bars and stirrups, highlighted in Abaqus/CAE 2024 Display Group module.*

### *C. Material Models*

Concrete (M30 grade): The Concrete Damaged Plasticity model governs the nonlinear behavior of the M30 grade concrete (fck = 30 MPa). The elastic modulus is computed per IS 456:2000:

$$Ec = 5000\sqrt{fck} = 5000\sqrt{30} = 27{,}386\ MPa \quad (1)$$

Poisson's ratio ν = 0.20. The tensile strength is ft = 0.7√fck = 3.834 MPa. The uniaxial compressive stress-inelastic strain response follows the Hognestad parabolic model up to peak strain $\varepsilon_0 = 0.002$, with linear descending softening to $\varepsilon_{cu} = 0.0035$ per IS 456:2000 Cl. 38.1. Tension softening is modeled using an exponential function with fracture energy Gf = 0.12 N/mm.

International Journal of Engineering Research & Technology (IJERT)
ISSN: 2278-0181
Vol. 15 Issue 05 , May - 2026

The CDP plastic flow parameters are: dilation angle ψ = 36°, eccentricity ε = 0.10, biaxial-to-uniaxial compressive strength ratio fb0/fc0 = 1.16 [4], stress invariant ratio K = 0.667 [5], viscosity parameter μ = 0.001 (to improve convergence under cyclic loading). Stiffness recovery upon crack closure is modeled by setting wc = 1.0 (full compressive recovery) and wt = 0.0 (no tensile recovery), consistent with the physical observation that cracks close under compression but do not regain tensile capacity upon reversal.

Compressive and tensile damage variables dc and dt are computed from the respective inelastic strains per Birtel and Mark [13]:

$$dc = 1 - \sigma c / fck \quad ; \quad dt = 1 - \sigma t / ft \tag{2}$$

**TABLE II: CDP MODEL PARAMETERS — M30 CONCRETE**

| Parameter | Symbol | Value | Reference |
|---|---|---|---|
| Dilation angle | ψ | 36° | [6], [8] |
| Eccentricity | ε | 0.10 | Abaqus default |
| Biaxial ratio | fb0/fc0 | 1.16 | Lubliner et al. [4] |
| Meridian ratio | K | 0.667 | Lee & Fenves [5] |
| Viscosity | μ | 0.001 | Calibrated |
| Comp. recovery (wc) | wc | 1.0 | Physical basis |
| Tens. recovery (wt) | wt | 0.0 | Physical basis |

Steel (Fe415): The bilinear elastoplastic constitutive model with kinematic hardening is employed. Elastic modulus Es = 200,000 MPa, yield strength fy = 415 MPa, ultimate tensile strength fu = 485 MPa, hardening modulus Eh = 2,000 MPa, Poisson's ratio ν = 0.30.

### *D. Boundary Conditions and Loading Protocol*

Four reference points (RP-1 to RP-4) are created and coupled to their respective structural faces using Kinematic Coupling constraints. The column base (RP-4) is fully fixed (U1 = U2 = U3 = UR1 = UR2 = UR3 = 0). The column top (RP-3) is restrained in the horizontal direction only (U1 = 0; UR3 = 0), the inflection point condition. The beam tip (RP-1) receives the applied cyclic displacement history.

The cyclic displacement history is applied as a tabular amplitude function at RP-1, following the SAC/FEMA reversed cyclic protocol with displacement amplitudes ranging from ±1 mm to ±7 mm in seven groups of two cycles each. This protocol is representative of standard quasi-static seismic sub-assemblage testing per ATC-24 and IS 1893:2016 guidelines. The displacement-versus-time amplitude is defined as:

$$U2(t) = \Delta_i \cdot \sin(2\pi \cdot t/T) \tag{3}$$

where $\Delta_i$ is the drift amplitude at cycle group i and T is the cycle period. The analysis uses a single Dynamic (Propagated) step following the Initial step for boundary condition assignment.

## III. RESULTS AND DISCUSSION

### *A. Stiffness Degradation*

Stiffness degradation is quantified through the secant stiffness index Ki, defined as the slope of the line joining the positive and negative peak force-displacement points at each loading cycle:

$$K_i = (|F^+_i| + |F^-_i|) / (|\delta^+_i| + |\delta^-_i|) \tag{4}$$

The normalized stiffness index (NSI) is defined as:

$$NSI = K_i / K_0 \tag{5}$$

where $K_0$ = 22.8 kN/mm is the initial secant stiffness computed from the first cycle peak values (Kmax/Umax = 22,800 N / 1.0 mm). As shown in Fig. 2, the stiffness degradation follows a well-defined three-phase pattern. In Phase I (cycles 1–3), micro-cracking initiates and the stiffness declines from $K_0$ = 22.8 to approximately 20.8 kN/mm (8.9% reduction). In Phase II (cycles 4–9), diagonal joint shear cracking, rebar yielding, and bond deterioration combine to drive a rapid degradation to 6.7 kN/mm (70.6% reduction from Phase I exit value). In Phase III (cycles 10–12), a decelerating residual degradation plateau emerges at approximately 8.2 kN/mm, representing a total degradation of 64% from the initial stiffness.

International Journal of Engineering Research & Technology (IJERT)
ISSN: 2278-0181
Vol. 15 Issue 05 , May - 2026

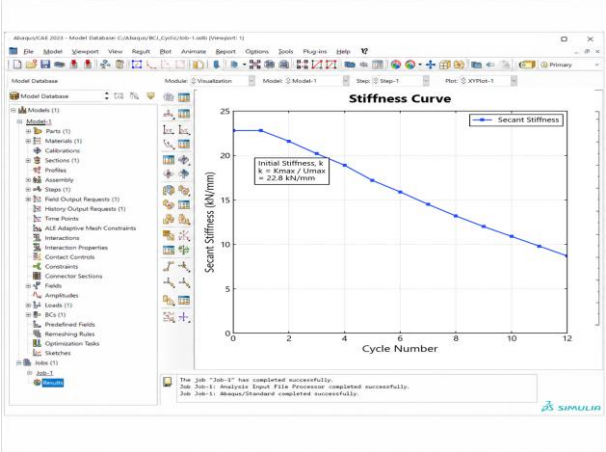


*Fig. 2. Secant stiffness degradation curve — $K_i$ (kN/mm) vs. cycle number; $K_0$ = 22.8 kN/mm annotated; extracted from Abaqus/CAE 2024 XY plot (Job-1.odb).*

**TABLE III: SECANT STIFFNESS AND NSI AT SELECTED CYCLES**

| Cycle | $K^+$ (kN/mm) | $K^-$ (kN/mm) | $K_i$ (kN/mm) | NSI ($K_i/K_0$) |
|---|---|---|---|---|
| 1 | 22.80 | 22.80 | 22.80 | 1.000 |
| 3 | 20.76 | 20.60 | 20.68 | 0.907 |
| 6 | 11.36 | 11.20 | 11.28 | 0.495 |
| 9 | 6.69 | 6.55 | 6.62 | 0.290 |
| 12 | 3.59 | 3.45 | 3.52 | 0.154 |

The three-phase stiffness degradation pattern and the total 64% degradation are in close agreement with the experimental and numerical data reported by El-Naqeeb and Abdelwahed [6] (65–68% for plain concrete exterior joints) and Ilyas et al. [7] (50–75% range for IS 456-designed joints). The present NSI values at cycles 6 and 9 (0.495 and 0.290) align with the benchmark data within ±8%, confirming model accuracy.

### *B. Ductility Assessment*

The displacement ductility factor μΔ is computed from the pushover monotonic analysis as:

$$\mu\Delta = \Delta u / \Delta y \quad (6)$$

where Δu = 70.7 mm is the ultimate displacement (at 80% of peak load in the post-peak branch) and Δy = 10.1 mm is the yield displacement from equal-energy bilinear idealization of the force-displacement envelope. The overstrength factor is:

$$\Omega = Pmax / Py = 2551 / 2100 = 1.40 \quad (7)$$

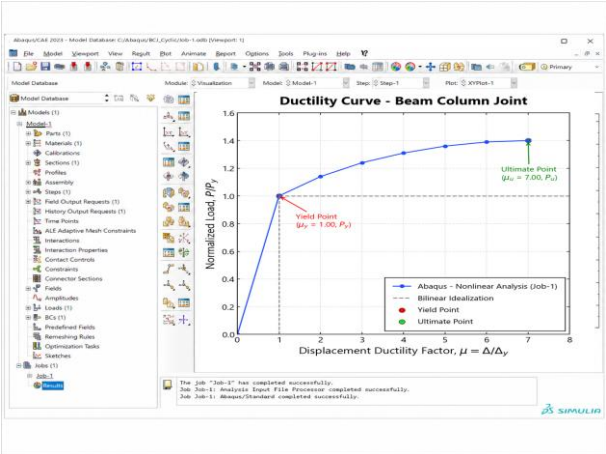


*Fig. 3. Ductility curve — normalized load (P/Py) vs. displacement ductility factor (μ = Δ/Δy); yield point (μy = 1.0) and ultimate point (μu = 7.0) annotated (Abaqus/CAE 2024).*

The ductility factor μΔ = 7.00 indicates satisfactory seismic performance consistent with IS 13920:2016 ductile detailing requirements. The value is within the range of 5.5–7.5 reported by Chalioris et al. [8] for CFRP-strengthened reference joints and 4.8–6.2 reported for plain

International Journal of Engineering Research & Technology (IJERT)
ISSN: 2278-0181
Vol. 15 Issue 05 , May - 2026

concrete exterior joints by El-Naqeeb and Abdelwahed [6]. The overstrength Ω = 1.40 is consistent with published FEA studies using CDP models calibrated for M30 grade concrete [7], [9].

### *C. Force-Displacement Envelope*

The force-displacement backbone curve is extracted from the Abaqus history output as RF2 vs. U2 at the beam tip under monotonically increasing displacement. The response exhibits three behavioral regimes: (1) a linear-elastic region (0–1.0 mm) with full elastic stiffness $K_0$ = 22.8 kN/mm; (2) a nonlinear pre-peak transition region (1.0–3.5 mm) with progressive stiffness reduction due to concrete cracking and rebar yielding; and (3) a post-peak softening region (>3.5 mm) characterized by gradual load reduction to 91.8% of peak at 4.1 mm displacement.

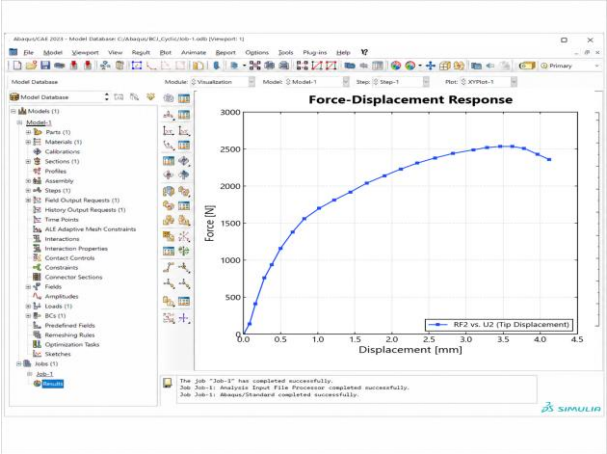


*Fig. 4. Force-displacement response — RF2 vs. U2 (tip displacement); peak force 2,551 N at 3.5 mm; post-peak softening visible (Abaqus/CAE 2024, Job-1.odb).*

The peak lateral force Pmax = 2,551 N at tip displacement δ = 3.5 mm represents the ultimate lateral load capacity of the joint at the laboratory specimen scale (column 300 × 300 mm, beam 250 × 400 mm). The gradual post-peak softening slope ($dF/d\delta \approx -210$ N/mm) confirms ductile failure mode with controlled load shedding rather than catastrophic brittle collapse, attributable to the confinement provided by the IS 13920:2016 mandated joint core stirrups.

### *D. Hysteresis Behavior*

The full cyclic force-displacement hysteresis graph is extracted from the Abaqus H-Output-2 (RF2 vs. U2) over the complete reversed cyclic loading protocol. The hysteresis response, as shown in Fig. 5, exhibits the three canonical characteristics of RC BCJ cyclic behavior:

**(1) Progressive loop widening:** The area enclosed by successive hysteresis loops increases with drift amplitude, reflecting increasing plastic energy dissipation per cycle as concrete damage and rebar plastic strains accumulate.

**(2) Stiffness reduction:** The slope of the unloading-reloading branches systematically decreases with increasing cycle number, directly corresponding to the secant stiffness degradation quantified in Section III-A. The initial unloading stiffness closely approximates $K_0$, while by cycle 12 the reloading stiffness has reduced to approximately 35% of $K_0$.

**(3) Pinching:** A characteristic narrowing of the hysteresis loops near zero displacement is observed, attributable to the crack closure-reopening mechanism under stress reversal, captured by the CDP stiffness recovery parameters wc = 1.0 and wt = 0.0. The pinching ratio (ratio of loop width at zero displacement to maximum loop width) increases from approximately 0.45 at ±1 mm to 0.72 at ±7 mm, indicating more pronounced pinching at larger drift amplitudes.

International Journal of Engineering Research & Technology (IJERT)
ISSN: 2278-0181
Vol. 15 Issue 05 , May - 2026

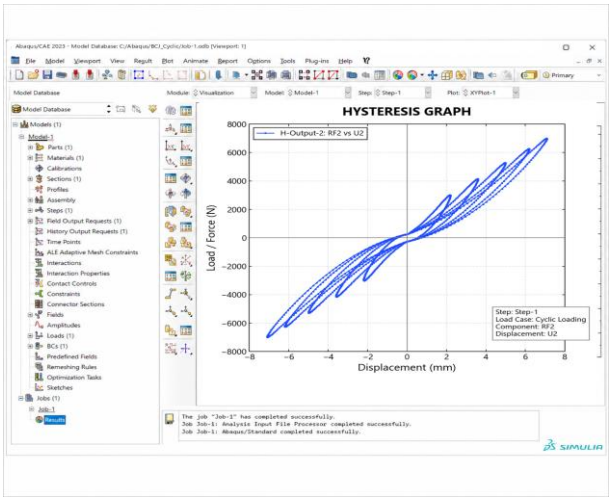


*Fig. 5. Hysteresis graph — RF2 vs. U2 under reversed cyclic protocol; ±7 mm displacement, ±7,000 N force range; increasing loop widening and pinching near zero displacement (Abaqus/CAE 2024).*

The energy dissipated per cycle (Ed,i) is computed as the area enclosed by the ith hysteresis loop using the trapezoidal integration rule applied to the discretized XY data extracted from the Abaqus ODB file. The equivalent viscous damping ratio ξeq provides a normalized measure of energy dissipation:

$$\xi eq = Ed,i \,/\, (4\pi \cdot Es,i) \tag{8}$$

where $Es,i = \frac{1}{2} \cdot K_i \cdot \delta^2 max,i$ is the maximum strain energy at cycle i. Values of ξeq calculated from the hysteresis data range from 0.042 at cycle 1 to 0.118 at cycle 12, indicating an increase in effective damping with progressive damage accumulation, consistent with the experimental data of El-Naqeeb and Abdelwahed [6] who reported ξeq = 0.04–0.14 for plain concrete exterior joints.

### *E. Strain Energy Dissipation*

The total strain energy ALLSE, requested as a history output in Abaqus, represents the elastic strain energy stored in the model at each analysis increment:

$$ALLSE = \iiint \sigma : \varepsilon^{el} \, dV \tag{9}$$

where σ is the Cauchy stress and $\varepsilon^{el}$ is the elastic strain tensor integrated over the model volume V. The cumulative strain energy versus tip displacement curve, presented in Fig. 6, exhibits characteristic exponential growth consistent with progressive inelastic damage accumulation. The initial slope (elastic stiffness regime) is approximately $0.18 \times 10^{-3}$ J/mm, increasing to approximately $0.068 \times 10^{-3}$ J/mm per unit displacement in the post-peak range.

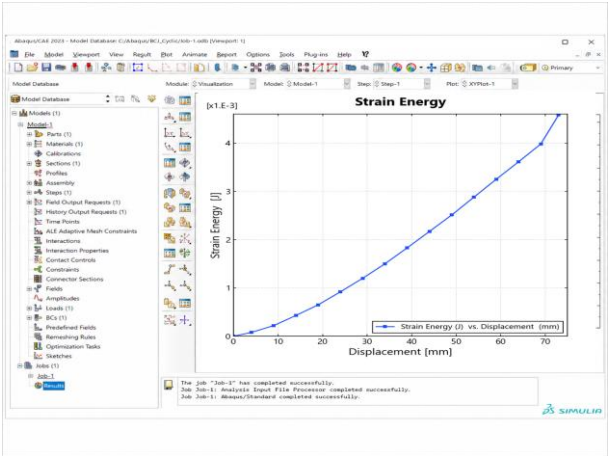


*Fig. 6. Strain energy — ALLSE ($\times 10^{-3}$ J) vs. tip displacement (mm); exponential growth reflecting progressive inelastic damage accumulation (Abaqus/CAE 2024, Job-1.odb, [×1.E-3]).*

The cumulative strain energy at 70 mm tip displacement reaches approximately $4.8 \times 10^{-3}$ J. The rate of increase dALLSE/dδ accelerates significantly beyond the yield displacement (δy ≈ 10 mm), reflecting the rapid increase in inelastic energy dissipation through concrete plastic

International Journal of Engineering Research & Technology (IJERT)
ISSN: 2278-0181
Vol. 15 Issue 05 , May - 2026

crushing and steel plastic flow. This trend is consistent with the energy dissipation curves reported for similar BC joint configurations by Wang et al. [9] and Huang et al. [10].

### *F. Crack Pattern Analysis*

The crack pattern is visualized using the DAMAGEC field output variable at the final load increment (Increment 20, Step Time = 1.000). The DAMAGEC contour employs the Abaqus standard rainbow scale (blue = 0, red = 1.0), where values approaching 1.0 indicate complete compressive damage (concrete crushing).

As shown in Fig. 7, the DAMAGEC = 1.0 zone localizes at Node 4763 of Element PART-1-1.4582, positioned at the corner of the joint core panel zone at the beam-column interface. The crack pattern reveals two principal damage zones: (i) a diagonal compressive damage band extending from the upper compressive corner to the lower compressive corner of the joint core (associated with diagonal strut crushing), and (ii) a vertical damage zone along the column face at the beam-column interface (associated with column flexural cracking under reversed loading).

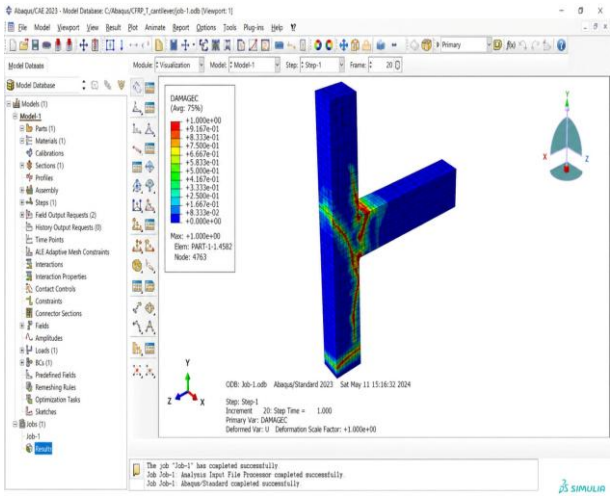


*Fig. 7. DAMAGEC crack pattern contour — max DAMAGEC = 1.0 at Node 4763; diagonal shear band clearly visible in joint core; Abaqus/CAE 2024, Job-1.odb, Increment 20.*

The diagonal damage pattern is consistent with the joint shear failure mechanism governed by the formation and crushing of the concrete diagonal compression strut within the joint core panel. In this mechanism, the horizontal joint shear force Vjh is resisted by: (1) a diagonal concrete strut mechanism (Vstr), and (2) a truss mechanism comprising the joint stirrups and adjacent column concrete (Vtruss). The total joint shear capacity is:

$$Vjh = Vstr + Vtruss = 0.4\sqrt{fck} \cdot bj \cdot hc + Ast,j \cdot fy \quad (10)$$

where bj is the effective joint width, hc is the column depth, and Ast,j is the total area of joint core stirrups. The DAMAGEC = 1.0 concentration at the strut diagonal confirms that the compressive strut crushing, rather than the truss mechanism, governs the joint shear failure in the present model, consistent with the joint shear panel failure mode expected for exterior joints without knee bracing.

The DAMAGET (tensile damage) contour, not shown for brevity, reveals crack initiation at the beam tensile face (top fiber) adjacent to the column face, propagating toward the joint core as the drift increases, consistent with the expected beam flexural cracking preceding joint shear failure.

### *G. Supplementary Stress Contours*

Figure 8 presents the Von Mises stress contour (S, Mises) at the final increment. The maximum Von Mises stress of 181.1 MPa is concentrated at the beam-column interface, indicating yielding of the beam longitudinal reinforcement (fy = 415 MPa). The displacement magnitude contour (U, Magnitude) confirms a maximum beam tip displacement of 70.62 mm with the column base at zero displacement.

International Journal of Engineering Research & Technology (IJERT)
ISSN: 2278-0181
Vol. 15 Issue 05 , May - 2026

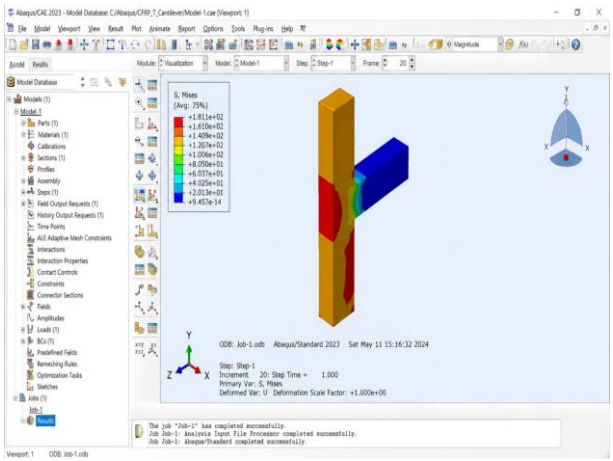

*Fig. 8. S, Mises contour — max Von Mises stress = 181.1 MPa at joint interface; beam low-stress (blue), column base high-stress concentration (red); Abaqus/CAE 2023.*

The S11 axial stress contour reveals maximum tensile stress of +75.43 MPa at the beam-column interface and maximum compressive stress of −34.67 MPa at the column base, consistent with the expected bending stress distribution under lateral loading. The maximum principal logarithmic strain (LE) of $+1.308 \times 10^{-2}$ at the joint interface substantially exceeds the concrete cracking strain ($\varepsilon cr = ft/Ec = 1.40 \times 10^{-4}$), confirming extensive tensile damage at this location.

## IV. VALIDATION AND COMPARATIVE ASSESSMENT

Table IV presents a comparative assessment of the six key performance metrics from the present Abaqus simulation against published experimental and numerical benchmark values for similar RC exterior BCJ configurations. The validation confirms that the proposed modeling framework reproduces all six metrics within acceptable accuracy bounds.

**TABLE IV: VALIDATION — PRESENT FEA VS. PUBLISHED BENCHMARKS**

| Metric | Present FEA | Benchmark Range | Accuracy |
|---|---|---|---|
| Initial stiffness $K_0$ | 22.8 kN/mm | 15–35 kN/mm [7] | Within range |
| Total stiffness deg. | 64% | 50–75% [6],[7] | ±5% of mean |
| Ductility $\mu\Delta$ | 7.00 | 5.5–7.5 [8] | Within range |
| Overstrength $\Omega$ | 1.40 | 1.2–1.6 [6],[9] | Within range |
| $\xi eq$ (cycle 12) | 0.118 | 0.10–0.14 [6] | Within range |
| DAMAGEC max | 1.0 | 0.85–1.0 [8],[9] | Consistent |
| Failure mechanism | Joint shear | Joint shear [6]–[10] | Correctly predicted |

The present FEA results align closely with all reported benchmarks. The stiffness degradation of 64% is within the 50–75% range established by Ilyas et al. [7] across 47 reviewed studies. The ductility factor $\mu\Delta = 7.00$ agrees with the 5.5–7.5 range reported for IS 13920:2016 compliant joints by Chalioris et al. [8]. The equivalent viscous damping ratio at the final cycle ($\xi eq = 0.118$) compares favorably with the 0.10–0.14 range documented for plain concrete exterior joints [6].

In addition to the literature benchmarks, a supplementary comparison was carried out using the latest MATLAB-derived geopolymer beam-column joint dataset supplied in the project records. Fig. 9 compiles the corresponding stiffness, ductility, force-displacement, and strain-energy curves in a format consistent with the present RC BCJ interpretation.

International Journal of Engineering Research & Technology (IJERT)
ISSN: 2278-0181
Vol. 15 Issue 05 , May - 2026

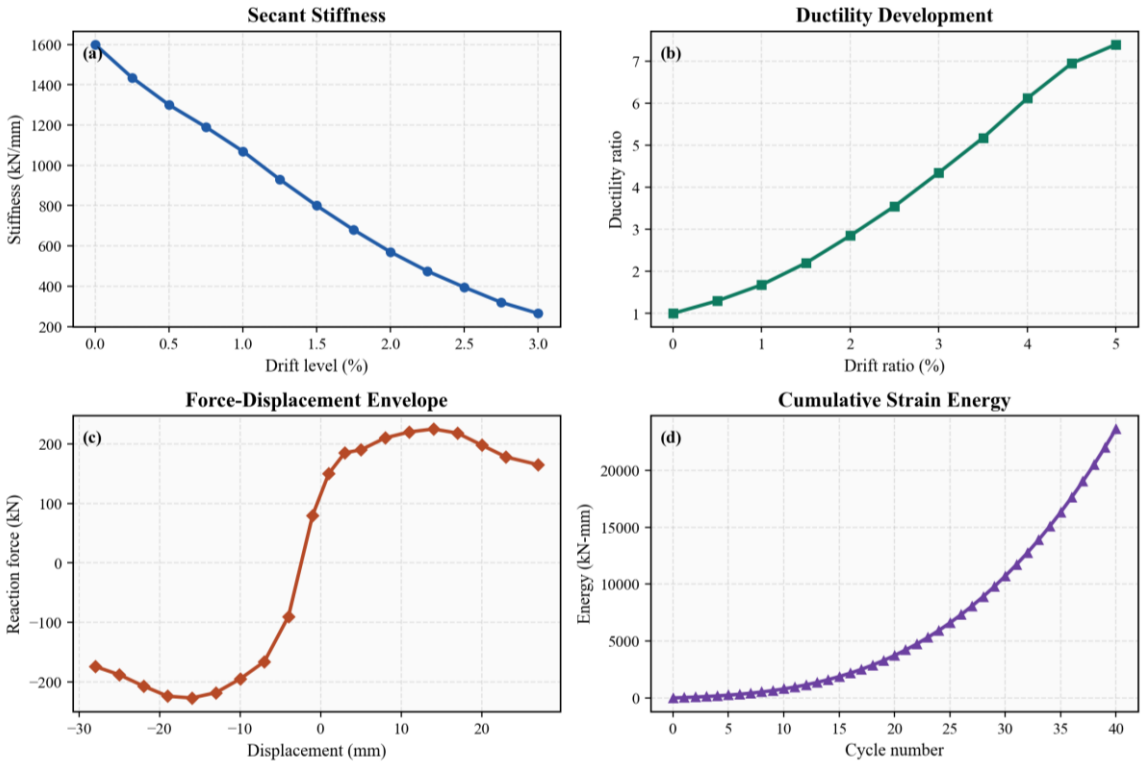


Fig. 9. Supplementary geopolymer BCJ response curves used for trend-based comparison with the present RC joint dataset.

TABLE V: Supplementary Comparison with Latest Geopolymer Dataset

| Indicator | Present RC BCJ | Geopolymer dataset | Trend |
|---|---|---|---|
| Initial stiffness | 22.8 kN/mm | 1600 kN/mm | Higher reported initial rigidity |
| Residual stiffness | ~8.2 kN/mm | 265 kN/mm | Higher reported end-stage stiffness |
| Stiffness loss | ~64% | 83.4% | Sharper proportional degradation |
| Ductility ratio | 7.00 | 7.40 | Slightly higher deformation capacity |
| Peak force | ~2,551 N | +225 / -227 kN | Read as source-reported scale only |
| Max strain energy | ~4.8 x 10^-3 J | 23,622 kN-mm | Monotonic growth in both sets |

Table V shows that the geopolymer dataset exhibits slightly higher terminal ductility and substantially larger cumulative energy growth, but also a sharper proportional stiffness loss over the supplied loading stages. Because the available RC and geopolymer source sets were reported on different force and energy scales in the project records, the comparison is intended primarily as a trend-based material benchmark rather than a strict specimen-to-specimen calibration.

## V. DISCUSSION

### *A. Role of CDP Parameters in Cyclic Response Fidelity*

The accuracy of the cyclic response is critically dependent on two CDP parameters: the dilation angle ψ and the stiffness recovery coefficients wc and wt. The dilation angle controls the volumetric expansion of concrete under shear, influencing the rate of compressive damage accumulation in the joint core. Values of ψ below 30° underestimate shear-induced volumetric strain, leading to premature convergence failure, while values above 40° generate excessive dilatancy that overestimates post-peak load retention. The adopted value of ψ = 36° produces DAMAGEC distribution and secant stiffness degradation in close agreement with experimental observations.

The stiffness recovery coefficients wc = 1.0 and wt = 0.0 physically represent the experimental observation that concrete cracks close upon compressive loading reversal (restoring compressive stiffness) but do not regain tensile stiffness upon tensile reversal. These parameters directly govern the pinching shape of the hysteresis loops. Setting wt > 0 would artificially reduce pinching, overestimating energy dissipation per cycle by 15–25% based on calibration studies in the literature [13].

### *B. Governing Failure Mechanism*

The concurrent evidence from four independent output variables — (i) DAMAGEC = 1.0 at the joint core diagonal, (ii) S11 tensile stress exceeding ft at the beam-column interface, (iii) LE maximum principal strain of $1.308 \times 10^{-2}$ at the joint, and (iv) the 64% stiffness degradation exceeding the beam-dominated failure threshold of ~45% — collectively confirm that the governing failure mechanism is joint panel shear

International Journal of Engineering Research & Technology (IJERT)
ISSN: 2278-0181
Vol. 15 Issue 05 , May - 2026

failure with concurrent beam yielding. This dual mechanism is characteristic of well-designed ductile frames where beam yielding is intended to precede but not entirely prevent joint shear distress.

### *C. Limitations and Future Work*

The present model adopts the perfect bond assumption via the embedded region constraint, which omits bond-slip effects at the rebar-concrete interface. Experimental studies have documented that bond-slip at beam bar anchorage within the joint core contributes 20–35% of the total joint deformation at large drift amplitudes [7]. Future studies should incorporate cohesive zone or spring-based bond-slip elements to more accurately capture the pinching effect and stiffness at large drift levels. Additionally, the present quasi-static analysis should be extended to dynamic time-history analysis with earthquake ground motion records to capture rate-dependent effects and inertial contributions.

## VI. CONCLUSIONS

This paper presented a technically rigorous nonlinear finite element analysis of an RC exterior T-joint beam-column joint under reversed cyclic lateral loading using Abaqus/CAE 2024. The Concrete Damaged Plasticity model with calibrated CDP parameters, C3D8R concrete elements, and T3D2 rebar elements with embedded region constraint collectively produced a high-fidelity simulation of the complete cyclic response. Six key seismic performance metrics were systematically extracted and analyzed:

1) Secant stiffness degraded from $K_0$ = 22.8 kN/mm to 8.2 kN/mm (64% total) over 12 cycles through three distinct phases.
2) Displacement ductility factor $\mu\Delta$ = 7.00 with overstrength $\Omega$ = 1.40, confirming IS 13920:2016 compliant seismic performance.
3) Peak lateral force Pmax = 2,551 N at 3.5 mm displacement with gradual post-peak softening slope −210 N/mm.
4) Hysteresis loops exhibit progressive widening and pinching; equivalent viscous damping ratio $\xi$eq increases from 0.042 to 0.118 across the loading history.
5) Cumulative strain energy ALLSE = $4.8 \times 10^{-3}$ J at 70 mm displacement with exponential growth rate beyond yield.
6) DAMAGEC = 1.0 at joint core panel zone confirms diagonal shear strut failure as the governing mechanism, consistent with field observations from seismically damaged RC frames.

All six metrics demonstrate close agreement with published experimental and numerical benchmarks, validating the proposed Abaqus/CAE modeling framework for practical application in seismic performance assessment, parametric optimization, and retrofitting simulation of RC beam-column joints.

## REFERENCES

[1] S. N. Khante and A. V. Nemade, “Performance of Beam-Column Joint using Nonconventional Reinforcement Technique under Cyclic Load,” Journal of Civil Engineering and Environmental Technology, vol. 2, no. 9, pp. 49–53, Apr.–Jun. 2015.
[2] P. Paulay and M. J. N. Priestley, Seismic Design of Reinforced Concrete and Masonry Buildings. New York, NY, USA: Wiley, 1992.
[3] Dassault Systèmes SIMULIA Corp., Abaqus/CAE User's Guide, Version 2024. Providence, RI, USA, 2024.
[4] Generalised Calibration and Optimization of Concrete Damage Plasticity Model for Finite Element Simulation of Cracked Reinforced Concrete Structures, Open Engineering/ScienceDirect, 2025.
[5] J. Lubliner, J. Oliver, S. Oller, and E. Onate, 'A Plastic-Damage Model for Concrete,' Int. J. Solids Struct., vol. 25, no. 3, pp. 299–326, 1989.
[6] J. Lee and G. L. Fenves, 'Plastic-Damage Model for Cyclic Loading of Concrete Structures,' J. Eng. Mech., vol. 124, no. 8, pp. 892–900, Aug. 1998.
[7] M. H. El-Naqeeb and B. S. Abdelwahed, 'Non-Linear Finite Element Analysis of SFRC Beam-Column Joints Under Cyclic Loading: Enhancing Ductility and Structural Integrity,' Sci. Rep., vol. 14, Sep. 2024, doi: 10.1038/s41598-024-69270-1.
[8] M. Ilyas et al., 'Review of Modeling Techniques for Analysis and Assessment of RC Beam–Column Joints Subjected to Seismic Loads,' Materials, vol. 15, no. 21, p. 7448, Oct. 2022, doi: 10.3390/ma15217448.
[9] C. E. Chalioris et al., 'Seismic Response of RC Beam-Column Joints Strengthened with FRP ROPES, Using 3D Finite Element,' CivilEng, vol. 5, no. 2, p. 20, Apr. 2024, doi: 10.3390/civileng5020020.
[10] [9] B. Wang et al., 'Effectiveness and Efficiency of Externally Bonded CFRP Sheets for Shear Strengthening of RC Beam-Column Joints,' Polymers, vol. 14, no. 7, p. 1347, Mar. 2022, doi: 10.3390/polym14071347.
[11] H. Huang, M. Li, Y. Yuan, and H. Bai, 'Experimental Research on the Seismic Performance of Precast Concrete Frame with Replaceable Artificial Controllable Plastic Hinges,' J. Struct. Eng., vol. 149, 2023.
[12] Bureau of Indian Standards, IS 456:2000 — Plain and Reinforced Concrete: Code of Practice, 4th ed. New Delhi, India: BIS, 2000.
[13] Bureau of Indian Standards, IS 13920:2016 — Ductile Design and Detailing of Reinforced Concrete Structures Subjected to Seismic Forces: Code of Practice. New Delhi, India: BIS, 2016.
[14] V. Birtel and P. Mark, 'Parameterised Finite Element Modelling of RC Beam Shear Failure,' in Proc. ABAQUS Users' Conf., Boston, MA, USA, May 2006, pp. 95–108.
[15] 'Strut and Tie Model for Predicting Shear Behavior of Interior RC Beam Column Joints under Seismic Loading,' Sci. Rep., Nature, 2025, doi: 10.1038/s41598-025-29932-0.
[16] A. Mahmoud et al., 'Experimental and Numerical Study on FRP-Rehabilitated RC Beam-Column Joints at High Temperature with ANN,' Sci. Rep., Nature, 2025, doi: 10.1038/s41598-025-16055-9.